Available online at www.sciencedirect.com
ScienceDirect
Physics Procedia 4 (2010) 89–105
Physics Procedia
www.elsevier.com/locate/procedia

Multi-dimensional multicanonical algorithm, simulated tempering, replica-exchange method, and all that

Ayori Mitsutake[a,1], Yoshiharu Mori[b,2], Yuko Okamoto[b,c,*]

[a]*Department of Physics, Keio University, Yokohama, Kanagawa 223-8522, Japan*
[b]*Department of Physics, Nagoya University, Nagoya, Aichi 464-8602, Japan*
[c]*Structural Biology Research Center, Nagoya University, Nagoya, Aichi 464-8602, Japan*

Abstract

We discuss multi-dimensional generalizations of multicanonical algorithm, simulated tempering, and replica-exchange method. We generalize the original potential energy function E_0 by adding any physical quantity V of interest as a new energy term with a coupling constant λ. We then perform a multi-dimensional multicanonical simulation where a random walk in E_0 and V space is realized. We can alternately perform a multi-dimensional simulated-tempering simulation where a random walk in temperature T and parameter λ is realized. The results of the multi-dimensional replica-exchange simulations can be used to determine the weight factors for these multi-dimensional multicanonical and simulated tempering simulations. Two examples of the above methods are presented for biomoleculr systems where the parameter λ corresponds to the solvation parameter and the pressure. In the former, a random walk in the conformational energy and solvation free energy is performed, and in the latter, a random walk in the potential energy and volume is realized.

Keywords: Generalized-ensemble algorithms, multicanonical algorithm, simulated tempering, replica-exchange method, parallel tempering, Mont Carlo, molecular dynamics

1. Introduction

Canonical fixed-temperature simulations of complex systems such as spin glasses and biopolymers are greatly hampered by the multiple-minima problem. Because simulations at low temperatures tend to get trapped in a few of a huge number of local-minimum-energy states which are separated by high-energy barriers, it is very difficult to obtain accurate canonical distributions at low temperatures by conventional Monte Carlo (MC) and molecular dynamics (MD)

*Corresponding author. *E-mail address:* okamoto@phys.nagoya-u.ac.jp
[1]*E-mail address:* ayori@mail.rk.phys.keio.ac.jp
[2]*E-mail address:* ymori@tb.phys.nagoya-u.ac.jp

1875-3892
doi:10.1016/j.phpro.2010.08.012

simulations. One way to overcome this multiple-minima problem is to perform a simulation in a *generalized ensemble* where each state is weighted by an artificial, non-Boltzmann probability weight factor so that a random walk in potential energy space may be realized (for reviews see, e.g., Refs. [1]–[5]). The random walk allows the simulation to overcome any energy barrier and to sample a much wider configurational space than by conventional methods. Monitoring the energy in a single simulation run, one can obtain not only the global-minimum-energy state but also canonical-ensemble averages as functions of temperature by the single-histogram [6] and/or multiple-histogram [7, 8] reweighting techniques (an extension of the multiple-histogram method is also referred to as the *weighted histogram analysis method* (WHAM) [8]).

Three of well-known generalized-ensemble algorithms are *multicanonical algorithm* (MUCA) [9, 10], *simulated tempering* (ST) [11, 12], and *replica-exchange method* (REM) [13, 14]. A powerful method closely related to MUCA is *Wang-Landau method* [15, 16]. ST is also referred to as the *method of expanded ensemble* [11]. The REM is also referred to as *parallel tempering* [17]. In MUCA, ST, and REM, random walks in potential energy (MUCA) and temperature (ST and REM) are realized.

The molecular dynamics version of MUCA was developed in Refs. [18, 19]. The details of molecular dynamics algorithm have also been worked out for REM in Ref. [20]. This led to a wide application of REM in the protein folding and related problems.

MUCA has been extended so that random walks in other parameters instead of energy may be obtained [21, 22, 23, 24, 25, 26, 27]. Moreover, two-dimensional (or two-component) extensions of MUCA can be found in Refs. [23, 24, 28, 29, 30]. One is also naturally led to a multi-dimensional (or, multivariable) extension of REM, which we refer to as *multi-dimensional replica-exchange method* (MREM) [31], where not only temperature but also other parameters of the system is exchanged in the replica-exchange process. An example of two-dimensional REM is temperature-pressure replica exchange [3, 32, 33]. The MREM formulation [31] led to many extensions of REM where parameters in the potential energy other than temperature (or special ensembles of the systems) are exchanged. Finally, ST can be extended to a multi-dimensional version as described below in detail.

In this article, we present general formulations of the multi-dimensional generalized-ensemble algorithms such as multi-dimensional MUCA, multi-dimensional ST, and multi-dimensional REM [34, 35, 36]. We generalize the original potential energy function E_0 by adding any physical quantities of interest V_ℓ as a new energy term with coupling constants $\lambda^{(\ell)}, (\ell = 1, \cdots, L)$. As an example of this general formulation, we describe generalized-ensemble algorithms in the isobaric-isothermal ensemble [37].

2. Methods

2.1. General formulations

We first give the general formulations for the multi-dimensional generalized-ensemble algorithms [34, 35, 36]. Let us consider a generalized potential energy function $E_{\boldsymbol{\lambda}}(x)$, which depends on L parameters $\boldsymbol{\lambda} = (\lambda^{(1)}, \cdots, \lambda^{(L)})$, of a system in state x. Although $E_{\boldsymbol{\lambda}}(x)$ can be any function of $\boldsymbol{\lambda}$, we consider the following specific generalized potential energy function:

$$E_{\boldsymbol{\lambda}}(x) = E_0(x) + \sum_{\ell=1}^{L} \lambda^{(\ell)} V_\ell(x) \, . \tag{1}$$

Here, there are $L+1$ energy terms, $E_0(x)$ and $V_\ell(x)$ ($\ell = 1, \cdots, L$), and $\lambda^{(\ell)}$ are the corresponding coupling constants for $V_\ell(x)$.

After integrating out the momentum degrees of freedom, the partition function of the system at fixed temperature T and parameters $\boldsymbol{\lambda}$ is given by

$$Z(T, \boldsymbol{\lambda}) = \int dx \exp(-\beta E_{\boldsymbol{\lambda}}(x)) = \int dE_0 dV_1 \cdots dV_L \, n(E_0, V_1, \cdots, V_L) \exp\left(-\beta E_{\boldsymbol{\lambda}}\right) , \quad (2)$$

where $n(E_0, V_1, \cdots, V_L)$ is the multi-dimensional density of states:

$$n(E_0, V_1, \cdots, V_L) = \int dx \delta(E_0(x) - E_0)\delta(V_1(x) - V_1) \cdots \delta(V_L(x) - V_L) , \quad (3)$$

$\beta = 1/k_{\mathrm{B}}T$, and k_{B} is the Boltzmann constant. Here, the integration is replaced by a summation when x is discrete.

The expression in Eq. (1) is often used in simulations. For instance, in simulations of spin systems, $E_0(x)$ and $V_1(x)$ (here, $L = 1$ and $x = \{S_1, S_2, \cdots\}$ stand for spins) can be respectively considered as the zero-field term and the magnetization term coupled with the external field $\lambda^{(1)}$. (For Ising model, $E_0 = -J \sum_{<i,j>} S_i S_j$, $V_1 = -\sum_i S_i$, and $\lambda^{(1)} = h$, i.e., external magnetic field.) In umbrella sampling [38] in molecular simulations, $E_0(x)$ and $V_\ell(x)$ can be taken as the original potential energy and the (biasing) umbrella potential energy, respectively, with the coupling parameter $\lambda^{(\ell)}$ (here, $x = \{\boldsymbol{q}_1, \cdots, \boldsymbol{q}_N\}$ where $\boldsymbol{q}_i$ are the coordinate vectors of the i-th particle and N is the total number of particles). For the molecular simulations in the isobaric-isothermal ensemble, $E_0(x)$ and $V_1(x)$ (here, $L = 1$) correspond respectively to the potential energy U and the volume $\mathcal{V}$ coupled with the pressure $\mathcal{P}$. (Namely, we have $x = \{\boldsymbol{q}_1, \cdots, \boldsymbol{q}_N, \mathcal{V}\}$, $E_0 = U$, $V_1 = \mathcal{V}$, and $\lambda^{(1)} = \mathcal{P}$, i.e., $E_{\boldsymbol{\lambda}}$ is the enthalpy without the kinetic energy contributions.) For simulations in the grand canonical ensemble with N particles, we have $x = \{\boldsymbol{q}_1, \cdots, \boldsymbol{q}_N, N\}$, and $E_0(x)$ and $V_1(x)$ (here, $L = 1$) correspond respectively to the potential energy U and the total number of particles N coupled with the chemical potential μ. (Namely, we have $E_0 = U$, $V_1 = N$, and $\lambda^{(1)} = -\mu$.)

Moreover, going beyond the well-known ensembles discussed above, we can introduce any physical quantity of interest (or its function) as the additional potential energy term V_ℓ. For instance, V_ℓ can be an overlap with a reference configuration in spin glass systems, an end-to-end distance, a radius of gyration in molecular systems, etc. In such a case, we have to carefully choose the range of $\lambda^{(\ell)}$ values so that the new energy term $\lambda^{(\ell)}V_\ell$ will have roughly the same order of magnitude as the original energy term E_0. We want to perform a simulation where a random walk not only in the E_0 space but also in the V_ℓ space is realized. As shown below, this can be done by performing a multi-dimensional MUCA, ST, or REM simulation.

The original MUCA can realize a one-dimensional random walk in potential energy space. The MUCA algorithms can be generalized to multi-dimensional ones. Here, we describe the multi-dimensional MUCA simulation which realizes a random walk in the $(L+1)$-dimensional space of $E_0(x)$ and $V_\ell(x)$ ($\ell = 1, \cdots, L$).

In the multi-dimensional MUCA ensemble, each state is weighted by the MUCA weight factor $W_{\mathrm{MU}}(E_0, V_1, \cdots, V_L)$ so that a uniform energy distribution of E_0, $V_1, \cdots$, and V_L may be obtained:

$$P_{\mathrm{MU}}(E_0, V_1, \cdots, V_L) \propto n(E_0, V_1, \cdots, V_L) W_{\mathrm{MU}}(E_0, V_1, \cdots, V_L) \equiv \mathrm{const} , \quad (4)$$

where $n(E_0, V_1, \cdots, V_L)$ is the multi-dimensional density of states. From this equation, we obtain

$$W_{\rm MU}(E_0, V_1, \cdots, V_L) \equiv \exp\left(-\beta_a E_{\rm MU}(E_0, V_1, \cdots, V_L)\right) \propto \frac{1}{n(E_0, V_1, \cdots, V_L)} , \tag{5}$$

where we have introduced an arbitrary reference temperature, $T_a = 1/k_{\rm B}\beta_a$, and wrote the weight factor in the Boltzmann-like form. Here, the "*multicanonical potential energy*" is defined by

$$E_{\rm MU}(E_0, V_1, \cdots, V_L) \equiv k_{\rm B} T_a \ln n(E_0, V_1, \cdots, V_L) . \tag{6}$$

The multi-dimensional MUCA MC simulation can be performed with the following Metropolis transition probability from state x with energy $E_{\boldsymbol{\lambda}} = E_0 + \sum_{\ell=1}^{L} \lambda^{(\ell)} V_\ell$ to state x' with energy $E_{\boldsymbol{\lambda}}{}' = E_0{}' + \sum_{\ell=1}^{L} \lambda^{(\ell)} V_\ell{}'$:

$$w(x \to x') = \min\left(1, \frac{W_{\rm MU}(E_0{}', V_1{}', \cdots, V_L{}')}{W_{\rm MU}(E_0, V_1, \cdots, V_L)}\right) = \min\left(1, \frac{n(E_0, V_1, \cdots, V_L)}{n(E_0{}', V_1{}', \cdots, V_L{}')}\right) . \tag{7}$$

An MD algorithm in the multi-dimensional MUCA ensemble also naturally follows from Eq. (5), in which a regular constant temperature MD simulation (with $T = T_a$) is performed by replacing the total potential energy $E_{\boldsymbol{\lambda}}$ by the multicanonical potential energy $E_{\rm MU}$ in the Newton's equations for the k-th particle ($k = 1, \cdots, N$) (see Refs. [18, 19] for the one-dimensional version):

$$\dot{\boldsymbol{p}}_k = - \frac{\partial E_{\rm MU}(E_0, V_1, \cdots, V_L)}{\partial \boldsymbol{q}_k} . \tag{8}$$

We now consider a multi-dimensional ST simulation which realizes a random walk both in temperature T and in parameters $\boldsymbol{\lambda}$. The entire parameter set $\boldsymbol{\Lambda} = (T, \boldsymbol{\lambda}) \equiv (T, \lambda^{(1)}, \cdots, \lambda^{(L)})$ become dynamical variables and both the configuration and the parameter set are updated during the simulation with a weight factor:

$$W_{\rm ST}(\boldsymbol{\Lambda}) \equiv \exp\left(-\beta E_{\boldsymbol{\lambda}} + f(\boldsymbol{\Lambda})\right) , \tag{9}$$

where the function $f(\boldsymbol{\Lambda}) = f(T, \boldsymbol{\lambda})$ is chosen so that the probability distribution of $\boldsymbol{\Lambda}$ is flat:

$$P_{\rm ST}(\boldsymbol{\Lambda}) \propto \int dE_0 dV_1 \cdots dV_L \; n(E_0, V_1, \cdots, V_L) \; \exp\left(-\beta E_{\boldsymbol{\lambda}} + f(\boldsymbol{\Lambda})\right) \equiv \text{const} . \tag{10}$$

This means that $f(\boldsymbol{\Lambda})$ is the dimensionless ("Helmholtz") free energy:

$$\exp\left(-f(\boldsymbol{\Lambda})\right) = \int dE_0 dV_1 \cdots dV_L \; n(E_0, V_1, \cdots, V_L) \; \exp(-\beta E_{\boldsymbol{\lambda}}) . \tag{11}$$

In the numerical work we discretize the parameter set $\boldsymbol{\Lambda}$ in $M(= M_0 \times M_1 \times \cdots \times M_L)$ different values: $\boldsymbol{\Lambda}_m \equiv (T_{m_0}, \boldsymbol{\lambda}_m) \equiv (T_{m_0}, \lambda_{m_1}^{(1)}, \cdots, \lambda_{m_L}^{(L)})$, where $m_0 = 1, \cdots, M_0, m_\ell = 1, \cdots, M_\ell$ ($\ell = 1, \cdots, L$). Without loss of generality we can order the parameters so that $T_1 < T_2 < \cdots < T_{M_0}$ and $\lambda_1^{(\ell)} < \lambda_2^{(\ell)} < \cdots < \lambda_{M_\ell}^{(\ell)}$ (for each $\ell = 1, \cdots, L$). The free energy $f(\boldsymbol{\Lambda}_m)$ is now written as $f_{m_0, m_1, \cdots, m_L} = f(T_{m_0}, \lambda_{m_1}^{(1)}, \cdots, \lambda_{m_L}^{(L)})$.

Once the initial configuration and the initial parameter set are chosen, the multi-dimensional ST is realized by alternately performing the following two steps:

1. A "canonical" MC or MD simulation at the fixed parameter set $\mathbf{\Lambda}_m = (T_{m_0}, \boldsymbol{\lambda}_m) = (T_{m_0}, \lambda^{(1)}_{m_1}, \cdots, \lambda^{(L)}_{m_L})$ is carried out for a certain steps with the weight factor $\exp(-\beta_{m_0} E_{\boldsymbol{\lambda}_m})$ (for fixed $\mathbf{\Lambda}_m$, $f(\mathbf{\Lambda}_m)$ in Eq. (9) does not contribute).
2. We update the parameter set $\mathbf{\Lambda}_m$ to a new parameter set $\mathbf{\Lambda}_{m\pm1}$ in which one of the parameters in $\mathbf{\Lambda}_m$ is changed to a neighboring value with the configuration and the other parameters fixed. The transition probability of this parameter updating process is given by the following Metropolis criterion:

$$w(\mathbf{\Lambda}_m \to \mathbf{\Lambda}_{m\pm1}) = \min\left(1, \frac{W_{\mathrm{ST}}(\mathbf{\Lambda}_{m\pm1})}{W_{\mathrm{ST}}(\mathbf{\Lambda}_m)}\right) = \min\left(1, \exp\left(-\Delta\right)\right) . \tag{12}$$

Here, there are two possibilities for $\mathbf{\Lambda}_{m\pm1}$, namely, T-update and $\lambda^{(\ell)}$-update. For T-update, we have $\mathbf{\Lambda}_{m\pm1} = (T_{m_0\pm1}, \boldsymbol{\lambda}_m)$ with

$$\Delta = \left(\beta_{m_0\pm1} - \beta_{m_0}\right) E_{\boldsymbol{\lambda}_m} - \left(f_{m_0\pm1,m_1,\cdots,m_L} - f_{m_0,m_1,\cdots,m_L}\right) . \tag{13}$$

For $\lambda^{(\ell)}$-update (for one of $\ell = 1, \cdots, L$), we have $\mathbf{\Lambda}_{m\pm1} = (T_{m_0}, \boldsymbol{\lambda}_{m_\ell\pm1})$ with

$$\Delta = \beta_{m_0}(E_{\boldsymbol{\lambda}_{m_\ell\pm1}} - E_{\boldsymbol{\lambda}_{m_\ell}}) - \left(f_{m_0,\cdots,m_\ell\pm1,\cdots} - f_{m_0,\cdots,m_\ell,\cdots}\right) , \tag{14}$$

where $\boldsymbol{\lambda}_{m_\ell\pm1} = (\cdots, \lambda^{(\ell-1)}_{m_{\ell-1}}, \lambda^{(\ell)}_{m_\ell\pm1}, \lambda^{(\ell+1)}_{m_{\ell+1}}, \cdots)$ and $\boldsymbol{\lambda}_{m_\ell} = (\cdots, \lambda^{(\ell-1)}_{m_{\ell-1}}, \lambda^{(\ell)}_{m_\ell}, \lambda^{(\ell+1)}_{m_{\ell+1}}, \cdots)$.

We remark that the random walk in β and in $\beta\lambda^{(\ell)}$ for the ST simulation corresponds to that in E_0 and in V_ℓ for the MUCA simulation:

$$\begin{cases} E_0 & \longleftrightarrow \beta , \\ V_\ell & \longleftrightarrow \beta\lambda^{(\ell)} , \quad (\ell = 1, \cdots, L) . \end{cases} \tag{15}$$

They are in conjugate relation.

2.2. Multi-dimensional replica-exchange method

We now describe the *multi-dimensional replica-exchange method* (MREM) [31] with the energy function given by Eq. (1). The system for the multi-dimensional REM consists of M non-interacting replicas of the original system in the "canonical ensemble" with $M(= M_0 \times M_1 \times \cdots \times M_L)$ different parameter sets $\mathbf{\Lambda}_m$ ($m = 1, \cdots, M$), where $\mathbf{\Lambda}_m = (T_{m_0}, \lambda^{(1)}_{m_1}, \cdots, \lambda^{(L)}_{m_L})$ and $m_0 = 1, \cdots, M_0, m_\ell = 1, \cdots, M_\ell$ ($\ell = 1, \cdots, L$). Because the replicas are non-interacting, the weight factor is given by the product of Boltzmann-like factors for each replica:

$$W_{\mathrm{MREM}} \equiv \prod_{m_0=1}^{M_0} \prod_{m_1=1}^{M_1} \cdots \prod_{m_L=1}^{M_L} \exp\left(-\beta_{m_0} E_{\boldsymbol{\lambda}_m}\right) . \tag{16}$$

REM closely follows the ST procedures described above. The multi-dimensional REM is realized by alternately performing the following two steps:

1. For each replica, a "canonical" MC or MD simulation at the fixed parameter set is carried out simultaneously and independently for a certain steps.

2. We exchange a pair of replicas i and j which are at the parameter sets $\mathbf{\Lambda}_m$ and $\mathbf{\Lambda}_{m+1}$, respectively. The transition probability for this replica exchange process is given by

$$w(\mathbf{\Lambda}_m \leftrightarrow \mathbf{\Lambda}_{m+1}) = \min\left(1, \exp(-\Delta)\right) \ , \tag{17}$$

where we have

$$\Delta = (\beta_{m_0} - \beta_{m_0+1})\left(E_{\boldsymbol{\lambda}_m}\left(q^{[j]}\right) - E_{\boldsymbol{\lambda}_m}\left(q^{[i]}\right)\right) \ , \tag{18}$$

for T-exchange, and

$$\Delta = \beta_{m_0}\left[\left(E_{\boldsymbol{\lambda}_{m_\ell+1}}(q^{[j]}) - E_{\boldsymbol{\lambda}_{m_\ell+1}}(q^{[i]})\right) - \left(E_{\boldsymbol{\lambda}_{m_\ell}}(q^{[j]}) - E_{\boldsymbol{\lambda}_{m_\ell}}(q^{[i]})\right)\right] \ , \tag{19}$$

for $\lambda^{(\ell)}$-exchange (for one of $\ell = 1, \cdots, L$). Here, $q^{[i]}$ and $q^{[j]}$ stand for configuration variables for replicas i and j, respectively, before the replica exchange.

Among the three algorithms described above, only MREM can be performed without much preparation because the weight factor for MREM is just a product of regular Boltzmann-like factors. On the other hand, we do not know the MUCA and ST weight factors *a priori* and need to estimate them. We proposed a powerful method for the weight factor determination in the one-dimensional MUCA and ST [39, 40, 41, 42, 43]. In this method, we use a short REM simulation and the multiple-histogram reweighting techniques. Here, we present our general formulation of the new method for the multi-dimensional case (see also Refs. [5]).

Suppose we have made a single run of a short multi-dimensional REM simulation with $M(= M_0 \times M_1 \times \cdots \times M_L)$ replicas that correspond to M different parameter sets $\mathbf{\Lambda}_m$ $(m = 1, \cdots, M)$. Let $N_{m_0,m_1,\cdots,m_L}(E_0, V_1, \cdots, V_L)$ and $n_{m_0,m_1,\cdots,m_L}$ be respectively the $(L+1)$-dimensional potential-energy histogram and the total number of samples obtained for the m-th parameter set $\mathbf{\Lambda}_m = (T_{m_0}, \lambda^{(1)}_{m_1}, \cdots, \lambda^{(L)}_{m_L})$. The generalized WHAM equations are then given by

$$n(E_0, V_1, \cdots, V_L) = \frac{\displaystyle\sum_{m_0,m_1,\cdots,m_L} N_{m_0,m_1,\cdots,m_L}(E_0, V_1, \cdots, V_L)}{\displaystyle\sum_{m_0,m_1,\cdots,m_L} n_{m_0,m_1,\cdots,m_L} \exp\left(f_{m_0,m_1,\cdots,m_L} - \beta_{m_0} E_{\boldsymbol{\lambda}_m}\right)} \ , \tag{20}$$

and

$$\exp(-f_{m_0,m_1,\cdots,m_L}) = \sum_{E_0,V_1,\cdots,V_L} n(E_0, V_1, \cdots, V_L) \exp\left(-\beta_{m_0} E_{\boldsymbol{\lambda}_m}\right) . \tag{21}$$

The density of states $n(E_0, V_1, \cdots, V_L)$ (which is inversely proportional to the multi-dimensional MUCA weight factor) and the dimensionless free energy $f_{m_0,m_1,\cdots,m_L}$ (which is the multi-dimensional ST parameter) are obtained by solving Eqs. (20) and (21) self-consistently by iteration.

We now present the equations to calculate ensemble averages of physical quantities with any temperature T and any parameter $\boldsymbol{\lambda}$ values. The expectation values of a physical quantity A at any T $(= 1/k_{\mathrm{B}}\beta)$ and any $\boldsymbol{\lambda}$ is given by

$$< A >_{T,\boldsymbol{\lambda}} = \frac{\displaystyle\sum_{E_0,V_1,\cdots,V_L} A(E_0, V_1, \cdots, V_L) n(E_0, V_1, \cdots, V_L) \exp\left(-\beta E_{\boldsymbol{\lambda}}\right)}{\displaystyle\sum_{E_0,V_1,\cdots,V_L} n(E_0, V_1, \cdots, V_L) \exp\left(-\beta E_{\boldsymbol{\lambda}}\right)} \ . \tag{22}$$

For the multi-dimensional MUCA simulation with the weight factor $W_{\rm MU}(E_0, \cdots, V_L)$, the best estimate of the density of states $n(E_0, V_1, \cdots, V_L)$ can be given by the single-histogram reweighting techniques. By substituting this quantity into Eq. (22), one can calculate the ensemble average of the physical quantity A as functions of T and $\boldsymbol{\lambda}$. Moreover, the ensemble average of the physical quantity A (including those that cannot be expressed as a function of E_0 and V_ℓ ($\ell = 1, \cdots, L$)) can be obtained as long as one stores the "trajectory" $A(x_k)$ from the production run, namely, we have

$$< A >_{T,\boldsymbol{\lambda}} = \frac{\sum_{x_k} A(x_k) \exp\left(-\beta(E_{\boldsymbol{\lambda}}(x_k)\right) W_{\rm MU}^{-1}(E_0(x_k), \cdots, V_L(x_k))}{\sum_{x_k} \exp\left(-\beta(E_{\boldsymbol{\lambda}}(x_k)\right) W_{\rm MU}^{-1}(E_0(x_k), \cdots, V_L(x_k))} . \tag{23}$$

Here, x_k is the configuration at the k th MC (or MD) step.

For the multi-dimensional ST or REM simulation, an ensemble average of the physical quantity A at any T and any $\boldsymbol{\lambda}$ is given by the multiple-histogram reweighting techniques as follows. In the ST or the REM simulation, we first obtain $N_{m_0,m_1,\cdots,m_L}(E_0, V_1, \cdots, V_L)$ and $n_{m_0,m_1,\cdots,m_L}$ in Eq. (20). The density of states $n(E_0, V_1, \cdots, V_L)$ and the dimensionless free energy $f_{m_0,m_1,\cdots,m_L}$ can then be obtained by solving Eqs. (20) and (21) self-consistently by iteration. Substituting the obtained density of states $n(E_0, V_1, \cdots, V_L)$ into Eq. (22), one can calculate the ensemble average of the physical quantity A at any T and any $\boldsymbol{\lambda}$.

Moreover, the ensemble average of the physical quantity A (including those that cannot be expressed as functions of E_0 and V_ℓ ($\ell = 1, \cdots, L$)) can be obtained from the "trajectory" of configurations of the production run [42]. Namely, we first obtain $f_{m_0,m_1,\cdots,m_L}$ ($m_0 = 1, \cdots, M_0, m_1 = 1, \cdots, M_1, m_L = 1, \cdots, M_L$) by solving Eqs. (20) and (21) self-consistently, and then we have

$$< A >_{T,\boldsymbol{\lambda}} = \frac{\sum_{n_0,n_1,\cdots,n_L} \sum_{x_k} A(x_k) \dfrac{\exp\left(-\beta E_{\boldsymbol{\lambda}}(x_k)\right)}{\sum_{m_0,m_1,\cdots,m_L} n_{m_0,m_1,\cdots,m_L} \exp\left(f_{m_0,m_1,\cdots,m_L} - \beta_{m_0} E_{\boldsymbol{\lambda}_m}(x_k)\right)}}{\sum_{n_0,n_1,\cdots,n_L} \sum_{x_k} \dfrac{\exp\left(-\beta E_{\boldsymbol{\lambda}}(x_k)\right)}{\sum_{m_0,m_1,\cdots,m_L} n_{m_0,m_1,\cdots,m_L} \exp\left(f_{m_0,m_1,\cdots,m_L} - \beta_{m_0} E_{\boldsymbol{\lambda}_m}(x_k)\right)}} , \tag{24}$$

where x_k are the configurations obtained at temperature T_{n_0} and $\boldsymbol{\lambda}_n$.

2.3. Multidimensional generalized-ensemble algorithms for the isobaric-isothermal ensemble

As an example of the general formulations in the previous subsection, we discuss the generalized-ensemble algorithms for isobaric-isothermal molecular simulations [37]. Let us consider a physical system that consists of N atoms and that is in a box of a finite volume V. The states of the system are specified by coordinates $r \equiv \{\boldsymbol{r}_1, \boldsymbol{r}_2, \cdots, \boldsymbol{r}_N\}$ and momenta $p \equiv \{\boldsymbol{p}_1, \boldsymbol{p}_2, \cdots, \boldsymbol{p}_N\}$ of the atoms and volume V of the box. The potential energy $E(r, V)$ for the system is a function of r and V.

We first describe MC simulation algorithms for MUCA, REM, and ST in the NPT ensemble. In these cases, momenta of atoms do not have to be considered. To make a system an equilibrium state, the detailed balance condition is imposed and a transition probability $w(X \to X')$ from an old state X to a new state X' can be given by the Metropolis criterion.

In MUBATH simulations, we introduce a function $\mathcal{H}(E, V)$ and use a weight factor $W_{\rm mbt}(E, V) \equiv \exp\left[-\beta_0 \mathcal{H}(E, V)\right]$ so that the distribution function $f_{\rm mbt}(E, V)$ of E and V may be uniform:

$$f_{\rm mbt}(E, V) \propto n(E, V) W_{\rm mbt}(E, V) = \text{constant}\,, \tag{25}$$

where β_0 is an arbitrary inverse reference temperature defined as $\beta_0 = 1/k_{\rm B}T_0$ ($k_{\rm B}$ is the Boltzmann constant) and $n(E, V)$ is the density of states.

To perform MUBATH MC simulations, the trial moves are generated in the same way as in the usual constant NPT MC simulations [44] and the transition probability from $X \equiv \{s, V\}$ to $X' \equiv \{s', V'\}$ is given by [45, 46]

$$w_{\rm mbt}(X \to X') = \min\left[1, \exp(-\Delta_{\rm mbt})\right], \tag{26}$$

where

$$\Delta_{\rm mbt} = \beta_0 \left\{\mathcal{H}\left[E(s', V'), V'\right] - \mathcal{H}\left[E(s, V), V\right] - N k_{\rm B} T_0 \ln(V'/V)\right\}, \tag{27}$$

and $s = \{\boldsymbol{s}_1, \boldsymbol{s}_2, \cdots, \boldsymbol{s}_N\}$ is the scaled coordinates defined by $\boldsymbol{s}_i = V^{-1/3}\boldsymbol{r}_i$ ($i = 1, 2, \cdots, N$). Here, we are assuming the box is a cube of side $V^{-1/3}$.

In REM simulations, we prepare a system that consists of $M_T \times M_P$ non-interacting replicas of the original system, where M_T and M_P are the number of temperature and pressure values used in the simulation, respectively. The replicas are specified by labels i ($i = 1, 2, \cdots, M_T \times M_P$), temperature by m_t ($m_t = 1, 2, \cdots, M_T$), and pressure by m_p ($m_p = 1, 2, \cdots, M_P$).

To perform REM MC (REMC) simulations, we carry out the following two steps alternately: (1) perform a usual constant NPT simulation in each replica at assigned temperature and pressure and (2) try to exchange the replicas. If the temperature (specified by m_t and n_t) and pressure (specified by m_p and n_p) between the replicas are exchanged, the transition probability from $X \equiv \{\cdots, (s^{[i]}, V^{[i]}; T_{m_t}, P_{m_p}), \cdots, (s^{[j]}, V^{[j]}; T_{n_t}, P_{n_p}), \cdots\}$ to $X' \equiv \{\cdots, (s^{[i]}, V^{[i]}; T_{n_t}, P_{n_p}), \cdots, (s^{[j]}, V^{[j]}; T_{m_t}, P_{m_p}), \cdots\}$ at the trial is given by [32, 3]

$$w_{\rm rem}(X \to X') = \min\left[1, \exp(-\Delta_{\rm rem})\right], \tag{28}$$

where

$$\Delta_{\rm rem} = (\beta_{m_t} - \beta_{n_t})\left[E(s^{[j]}, V^{[j]}) - E(s^{[i]}, V^{[i]})\right] + (\beta_{m_t} P_{m_p} - \beta_{n_t} P_{n_p})\left(V^{[j]} - V^{[i]}\right). \tag{29}$$

In ST simulations, we introduce a function $g(T, P)$ and use a weight factor $W_{\rm st}(E, V; T, P) \equiv \exp[-\beta(E + PV) + g(T, P)]$ so that the distribution function $f_{\rm st}(T, P)$ of T and P may be uniform:

$$f_{\rm st}(T, P) \propto \int_0^\infty dV \int_V dr\; W_{\rm st}[E(r, V), V; T, P] = \text{constant}\,. \tag{30}$$

From eq. (30), it is found that $g(T, P)$ is formally given by

$$g(T, P) = -\ln\left\{\int_0^\infty dV \int_V dr \exp\left[-\beta\left(E(r, V) + PV\right)\right]\right\}, \tag{31}$$

and the function is the dimensionless Gibbs free energy except for a constant.

To perform ST MC simulations, we carry out the following two steps alternately: (1) perform a usual constant NPT simulation and (2) try to update the temperature and pressure.

been determined before the simulation. The transition probability from $X \equiv \{s, V; T, P\}$ to $X' \equiv \{s, V; T', P'\}$ for this trial is given by

$$w_{\rm st}(X \to X') = \min\left[1, \exp(-\Delta_{\rm st})\right], \tag{32}$$

where

$$\Delta_{\rm st} = (\beta' - \beta)E(s, V) + (\beta' P' - \beta P)V - \left[g(T', P') - g(T, P)\right]. \tag{33}$$

For MD simulations with MUCA, REM, and ST in the NPT ensemble, the actual formulations depend on constant temperature and pressure algorithms. Here, we employ the MD methods with the Martyna-Tobias-Klein (MTK) algorithm, [47] whose equations of motion follow Nosé [48, 49] and Hoover [50] for the thermostat and Andersen [51] for the barostat.

To perform MUBATH MD simulations, we solve the usual equations of motion for the MTK algorithm except that it is necessary to modify the equations for $\boldsymbol{p}_i$ and p_ε as follows:

$$\begin{aligned} \frac{d\boldsymbol{p}_i}{dt} &= -\frac{\partial \mathcal{H}}{\partial E}\frac{\partial E}{\partial \boldsymbol{r}_i} - \left(1 + \frac{1}{N}\right)\frac{p_\varepsilon}{W}\boldsymbol{p}_i - \frac{p_\xi}{Q}\boldsymbol{p}_i\,, \\ \frac{dp_\varepsilon}{dt} &= 3V\left(P_{\rm int} - \frac{\partial \mathcal{H}}{\partial V}\right) + \frac{1}{N}\sum_{i=1}^{N}\frac{\boldsymbol{p}_i^2}{m_i} - \frac{p_\xi}{Q}p_\varepsilon\,, \end{aligned} \tag{34}$$

where

$$P_{\rm int} = \frac{1}{3V}\left[\sum_{i=1}^{N}\frac{\boldsymbol{p}_i^2}{m_i} - \frac{\partial \mathcal{H}}{\partial E}\left(\sum_{i=1}^{N}\boldsymbol{r}_i \cdot \frac{\partial E}{\partial \boldsymbol{r}_i} + 3V\frac{\partial E}{\partial V}\right)\right], \tag{35}$$

p_ε is the momentum associated with the logarithm of V, p_ξ is the momentum of the thermostat, and W and Q are the masses of barostat and thermostat, respectively.

When we perform MD simulations with REM and ST, the momenta should be rescaled if the replicas are exchanged for the temperature in REM [20] and the temperature is updated in ST [35].

3. Results

We tested the effectiveness of the new algorithms by using a system of a 17-residue fragment of ribonuclease T_1 [52, 42]. It is known by experiments that this peptide fragment forms α-helical conformations [52]. We have performed a two-dimensional REM simulation and a two-dimensional ST simulation. In these simulations, we used the following energy function:

$$E_\lambda = E_0 + \lambda E_{\rm SOL}\,, \tag{36}$$

where we set $L = 1, V_1 = E_{\rm SOL}$, and $\lambda^{(1)} = \lambda$ in Eq. (1). Here, E_0 is the potential energy of the solute and $E_{\rm SOL}$ is the solvation free energy. The parameters in the conformational energy as well as the molecular geometry were taken from ECEPP/2 [53, 54, 55].

The solvation term $E_{\rm SOL}$ is given by the sum of terms that are proportional to the solvent-accessible surface area of heavy atoms of the solute [56]. For the calculations of solvent-accessible surface area, we used the computer code NSOL [57].

The computer code KONF90 [58, 59] was modified in order to accommodate the generalized-ensemble algorithms. The simulations were started from randomly generated conformations. We prepared eight temperatures (M_0 =8) which are distributed exponentially between T_1 = 300 K

and T_{M_0} = 700 K (i.e., 300.00, 338.60, 382.17, 431.36, 486.85, 549.49, 620.20, and 700.00 K) and four equally-spaced λ values (M_1 = 4) ranging from 0 to 1 (i.e., $\lambda_1 = 0$, $\lambda_2 = 1/3$, $\lambda_3 = 2/3$, and $\lambda_4 = 1$) in the two-dimensional REM simulation and the two-dimensional ST simulation. Simulations with $\lambda = 0$ (i.e., $E_\lambda = E_0$) and with $\lambda = 1$ (i.e., $E_\lambda = E_0 + E_{\rm SOL}$) correspond to those in gas phase and in aqueous solution, respectively.

We first present the results of the two-dimensional REM simulation. We used 32 replicas with the eight temperature values and the four λ values given above. Before taking the data, we made the two-dimensional REM simulation of 100,000 MC sweeps with each replica for thermalization. We then performed the two-dimensional REM simulation of 1,000,000 MC sweeps for each replica to determine the weight factor for the two-dimensional ST simulation. At every 20 MC sweeps, either T-exchange or λ-exchange was tried (the choice of T or λ was made randomly). In each case, either set of pairs of replicas ((1,2),...,(M−1,M)) or ((2,3),...,(M,1)) was also chosen randomly, where M is M_0 and M_1 for T-exchange and λ-exchange, respectively.

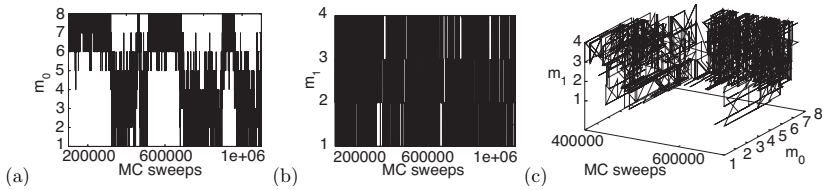

Figure 1: Time series of the labels of T_{m_0}, m_0, (a) and λ_{m_1}, m_1, (b) as functions of MC sweeps, and that of both T_{m_0} and λ_{m_1} for the region from 400,000 MC sweeps to 700,000 MC sweeps (c). The results were from one of the replicas (Replica 1). In (a) and (b), MC sweeps start at 100,000 and end at 1,100,000 because the first 100,000 sweeps have been removed from the consideration for thermalization purpose.

In Fig. 3 we show the time series of labels of T_{m_0} (i.e., m_0) and λ_{m_1} (i.e., m_1) for one of the replicas. The replica realized a random walk not only in temperature space but also in λ space. The behavior of T and λ for other replicas was also similar (data not shown). From Fig. 3, one finds that the λ-random walk is more frequent than the T-random walk.

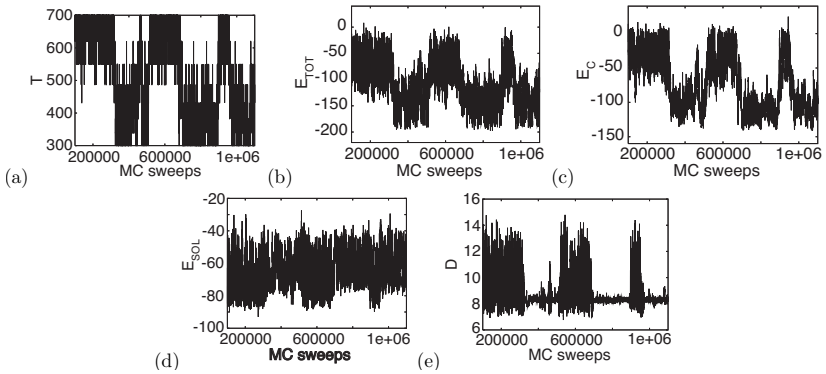

Figure 2: Time series of the temperature T (a), total energy $E_{\rm TOT}$ (b), conformational energy $E_{\rm C}$ (c), solvation free energy $E_{\rm SOL}$ (d), and end-to-end distance D (e) for the same replica as in Fig. 3. The temperature is in K, the energy is in kcal/mol, and the end-to-end distance is in Å.

We also show the time series of temperature T, total energy E_{TOT}, conformational energy E_{C}, solvation free energy E_{SOL}, and end-to-end distance D for the same replica in Fig. 3. From Figs. 3(a) and 3(e), we find that at lower temperatures the end-to-end distance is about 8 Å, which is the length of a fully α-helical conformation and that at higher temperatures it fluctuates much for a range from 7 Å to 14 Å. It suggests that α-helix structures exist at low temperatures and random-coil structures occur at high temperatures. There are transitions from/to α-helix structures to/from random coils during the simulation. It indicates that the REM simulation avoided getting trapped in local-minimum-energy states and sampled a wide configurational space.

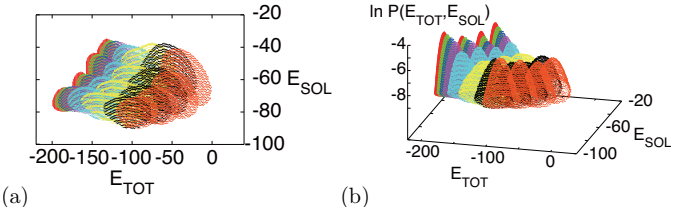

Figure 3: Contour curves and histograms of distributions of the total energy E_{TOT} and the solvation free energy E_{SOL} ((a) and (b)) from the two-dimensional REM simulation.

The canonical probability distributions of E_{TOT} and E_{SOL} at the 32 conditions obtained from the two-dimensional REM simulation are shown in Fig. 3. For an optimal performance of the REM simulation, there should be enough overlaps between all pairs of neighboring distributions, which will lead to sufficiently uniform and large acceptance ratios of replica exchanges. There are indeed ample overlaps between the neighboring distributions in Fig. 3.

We now use the results of the two-dimensional REM simulation to determine the weight factors for the two-dimensional ST simulation by the multiple-histogram reweighting techniques. Namely, by solving the generalized WHAM equations in Eqs. (20) and (21) with the obtained histograms at the 32 conditions (see Fig. 3), we obtained 32 values of the ST parameters $f_{m_0,m_1}(m_0 = 1,\cdots,8; m_1 = 1,\cdots,4)$.

After obtaining the ST weight factors, $W_{ST} = \exp(-\beta_{m_0}(E_{\mathrm{C}} + \lambda_{m_1} E_{\mathrm{SOL}}) + f_{m_0,m_1})$, we carried out the two-dimensional ST simulation of 1,000,000 MC sweeps for data collection after 100,000 MC sweeps for thermalization. At every 20 MC sweeps, either T_{m_0} or λ_{m_1} was respectively updated to $T_{m_0\pm1}$ or $\lambda_{m_1\pm1}$ (the choice of T or λ update and the choice of ±1 were made randomly).

We show the average total energy, average conformational energy, average $\lambda \times E_{\mathrm{SOL}}$, and average end-to-end distance in Fig. 3. The results are in good agreement with those of the REM simulation (data not shown).

We find that the results of the two-dimensional ST simulation are in complete agreement with those of the two-dimensional REM simulation for the average quantities. The only difference between the two simulations is the number of replicas. In the present simulation, while the REM simulation used 32 replicas, the ST simulation used only one replica. Hence, we can save much computer power with ST.

We now discuss the results of the simulations in detail with respect to the solvent effects. We found above that the results of both REM and ST simulations were essentially identical. Thus, in the following, we describe only the results of the two-dimensional REM simulation because it had 32 times more data than the ST case.

We compare the conformations obtained with $\lambda = 0$ (in gas phase) and those with $\lambda = 1$

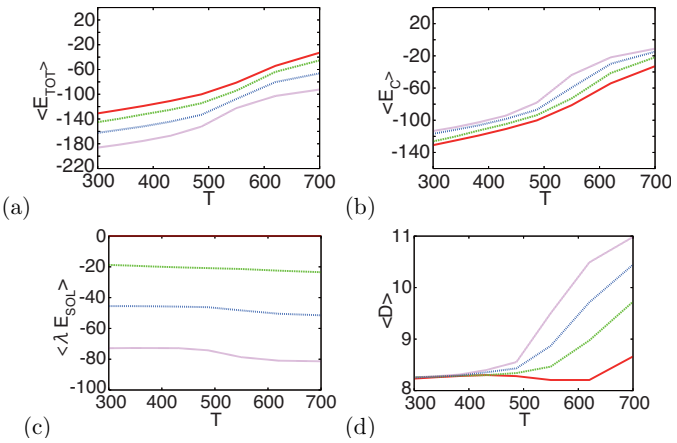

Figure 4: The average total energy (a), average conformational energy (b), average of $\lambda \times E_{\mathrm{SOL}}$ (c), and average end-to-end distance (d) with all the λ values as functions of temperature. The lines colored in red, green, blue, and purple are for λ_1, λ_2, λ_3, and λ_4, respectively.

(in aqueous solution) at the lowest temperature (300 K). Most conformations were complete α-helix structures in both cases for all the MC sweeps (data not shown). The backbones of the two conformations are essentially identical. However, some side-chain conformations are different.

The atoms located on the side chains can make hydrogen bonds with water molecules. The heavy atoms preferred to make interactions with water atoms because the atomistic solvation free energy decreased as the accessible surface area increased. The arrangements of side chains of the heavy atoms occurred in aqueous solution so that their accessible surface areas increased (i.e., to expose to water). It implies that at low temperatures, a random walk in λ space causes the change of side-chain structures because of the solvent effects, while the backbone remains almost identical (α-helix structure).

Moreover, we compare the conformations with $\lambda = 0$ (in gas phase) and those with $\lambda = 1$ (in aqueous solution) at the highest temperature T_8. The snapshots of the conformations at 200,000 MC sweeps, 600,000 MC sweeps, and 1,000,000 MC sweeps in gas phase and in aqueous solution are shown in Fig. 3. Although all structures are extended and in random-coil state due to entropic effects, there are different characteristics of the conformations in gas phase and in aqueous solution. The conformations in gas phase seem to be slightly more compact than those in aqueous solution. The end-to-end distance in gas phase was also smaller than that in aqueous solution. In aqueous solution, charged atoms prefer to make interactions with water molecules and thus there are less intra-chain interactions. As a result, the conformations in aqueous solution are more extended than those in gas phase at the same temperature. These results are also supported by the behavior of the solvation free energy in Fig. 3(a) and the end-to-end distance in Fig. 3(d). At high temperatures, it implies that both structures are random coils but a random walk of λ space causes to change structures from/to a slightly compact ones to/from extended ones.

In order to verify that the generalized-ensemble algorithms in the isobaric-isothermal ensemble discussed above can be effective for conformational sampling and give the same results, we performed MD simulations with the three generalized-ensemble algorithms. We used a system

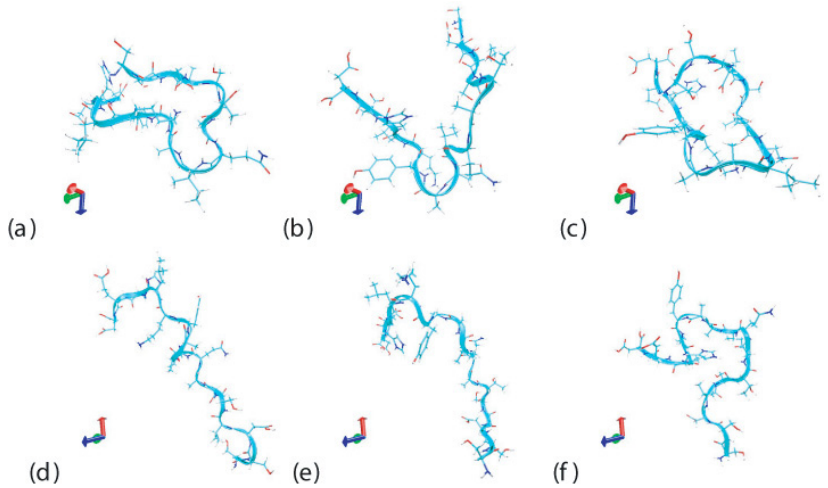

Figure 5: Snapshots at 200,000 MC sweeps ((a) and (d)), at 600,000 MC sweeps ((b) and (e)), and at 1,000,000 MC sweeps ((c) and (f)) at the highest temperature T_8. (a), (b), and (c) correspond to $\lambda = 0$ (in gas phase) and (d), (e), and (f) to $\lambda = 1$ (in aqueous solution). VMD software [60] and Raster 3D software [61] were used to create the figures.

of an alanine dipeptide in 73 surrounding water molecules and the system was placed in a cubic cell with periodic boundary conditions. Both of the backbone dihedral angles ϕ and ψ of the peptide were initially set to 180°. The simulations were performed with the program package. [62] several of the programs were modified and a few programs were added so that MUBATH, REM, and ST simulations with the MTK algorithm can be performed. We used the AMBER parm99 force field [63] for the peptide and the TIP3P water model. [64] The electrostatic interactions were calculated by the particle mesh Ewald method. [65, 66] In the van der Waals interaction calculations, we used the spherical cutoff method and the cutoff distance was set to 12.0 Å. The integration of the equations of motion was employed by the method proposed by Martyna *et al.* [67] and the Shake/Rattle/Roll constraint method [68, 69, 67] was used so that the water molecules are rigid body molecules. The unit time step was set to 0.5 fs. The mass parameters W and Q were determined as in ref. [67].

First, we performed the two-dimensional REMD simulation. The simulation time was set to 2.0 ns. We used the following 6 temperature $(T_1, \cdots, T_6)$ and 4 pressure $(P_1, \cdots, P_4)$ values: 280, 305, 332, 362, 395, and 430 K for temperature and 0.1, 65, 150, and 250 MPa for pressure. At the replica-exchange trial, either exchanging temperature (T-exchange) or exchanging pressure (P-exchange) was chosen randomly and then the pairs $\{(T_1, T_2), (T_3, T_4), (T_5, T_6)\}$ or $\{(T_2, T_3), (T_4, T_5)\}$ for T-exchange and $\{(P_1, P_2), (P_3, P_4)\}$ or $\{(P_2, P_3)\}$ for P-exchange were also chosen randomly.

We then performed 24 MUBATH simulations of 2.0 ns, where the total simulation time was 48 ns so that it is equal to that in the REMD simulation. In each of the simulations, different initial velocities were given. The data were sampled every 100 fs. The reference temperature was set to 430 K.

Figure 6 shows the probability distributions of E and V from the MUBATH simulations. From Fig. 6(a), it is found that the MUBATH simulations gave a uniform distribution in the

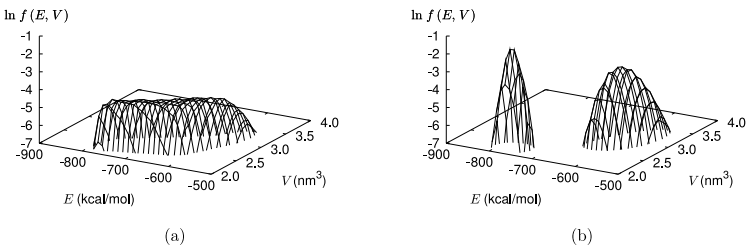

Figure 6: Logarithm of probability distributions f of E and V (a) in the MUBATH simulations and (b) for the NPT ensemble at 280 K and 250 MPa (left) and at 430 K and 0.1 MPa (right). The distributions corresponding to the NPT ensemble were calculated by the single-histogram reweighting techniques [6] using the results of the MUBATH simulations.

range where the density of states was obtained accurately in the REMD simulation and that the distribution of the MUBATH simulations was much wider than the ones for the NPT ensemble (see Fig. 6(b)).

Twenty-four ST simulations of 2.0 ns were carried out, which gave us the same number of sampled data as in the REMD and MUBATH simulations. In each simulation, different initial velocities were given. We used the same temperature and pressure values as in the REMD simulation. We tried to update the parameter (T or P) every 100 fs and the data were sampled just before the trials. The choice between updating T (T-update) and updating P (P-update) was made randomly and then either T_{m_t-1} or T_{m_t+1} for T-update and P_{m_p-1} or P_{m_p+1} for P-update was also chosen randomly, where m_t and m_p stand for the labels corresponding to the temperature and the pressure before the trial, respectively.

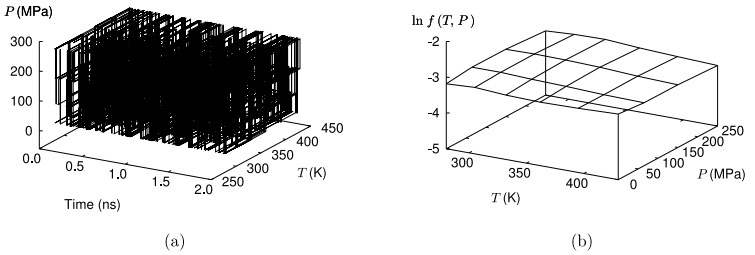

Figure 7: Results of the ST simulations: (a) the time series of T and P for 2.0 ns and (b) the logarithm of the probability distribution f of T and P.

Figure 7(a) shows the time series of T and P and Fig. 7(b) shows the probability distribution of T and P. These figures indicate that random walks in T-P space were successfully realized. The acceptance ratios in the ST simulations were in the range from 0.260 to 0.430 for T-update and from 0.426 to 0.642 for P-update, respectively.

Figure 8 shows the probability distributions of the backbone dihedral angles at 298 K and 0.1 MPa in all the simulations. Compared with the simulations with REMD, MUBATH, and ST, we also performed 24 conventional isobaric-isothermal simulations of 2.0 ns at 298 K and 0.1 MPa with different initial velocities. The dihedral angle distributions in the simulations with

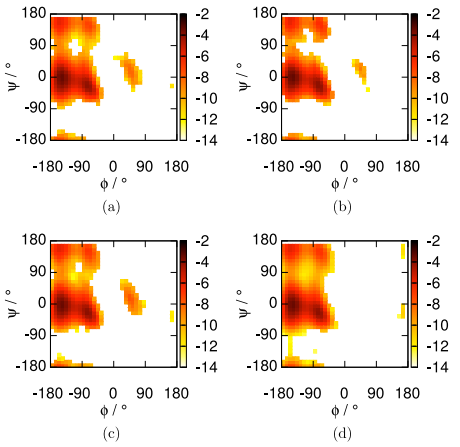

Figure 8: Contour maps of probability distribution of the backbone dihedral angles ϕ and ψ in the simulations with (a) REMD, (b) MUBATH, and (c) ST and (d) in the conventional isobaric-isothermal simulations. In these figures, the probability distributions at 298 K and 0.1 MPa are plotted in logarithmic scale and were calculated by the single-histogram reweighting techniques for MUBATH and by WHAM for REMD and ST.

the generalized-ensemble algorithms had a small peak in $0^\circ \leq \phi \leq 90^\circ$ and $-90^\circ \leq \psi \leq 90^\circ$, although there was no peak in the range in the distribution of the conventional simulations. All the simulations with the three generalized-ensemble algorithms were able to provide the same results and reproduce the distribution obtained previously in Refs. [70] and [71].

4. Conclusions

In this article we presented the general formulations of the multi-dimensional MUCA, ST, and REM. We generalized the original potential energy function E_0 by adding any physical quantities V_ℓ of interest as a new energy term with a coupling constant $\lambda^{(\ell)}(\ell = 1, \cdots, L)$. The simulation in multi-dimensional MUCA algorithms realizes a random walk in $E_0, V_1, \cdots, V_L$ spaces. On the other hand, the simulations in multi-dimensional ST algorithms and multi-dimensional REM realize a random walk in temperature and $\lambda^{(\ell)}(\ell = 1, \cdots, L)$ spaces.

While the multi-dimensional REM simulation can be easily performed because no weight factor determination is necessary, the required number of replicas can be quite large and computationally demanding. We thus prefer to use the multi-dimensional MUCA or ST, where only a single replica is simulated, instead of REM. However, it is very difficult to obtain optimal weight factors for the multi-dimensional MUCA and ST. Here, we have proposed a powerful method to determine these weight factors. Namely, we first perform a short multi-dimensional REM simulation and use the multiple-histogram reweighting techniques to determine the weight factors for multi-dimensional MUCA and ST simulations.

The multi-dimensional generalized-ensemble algorithms that were presented in the present article will be very useful for Monte Carlo and molecular dynamics simulations of complex systems such as spin glass, molecular, polymer, and biopolymer systems.

Acknowledgements:
Some of the results were obtained by the computations on the super computers at the Institute

for Molecular Science, Okazaki, Japan. This work was supported, in part, by Grants-in-Aid for Scientific Research in Priority Areas ("Water and Biomolecules" and "Molecular Theory for Real Systems"), for Scientific Research on Innovative Areas ("Fluctuations and Biological Functions"), and for the Next Generation Super Computing Project, Nanoscience Program from the Ministry of Education, Culture, Sports, Science and Technology (MEXT), Japan.

References

[1] U.H.E. Hansmann and Y. Okamoto, in *Annual Reviews of Computational Physics VI*, edited by D. Stauffer (World Scientific, Singapore, 1999) pp. 129–157.
[2] A. Mitsutake, Y. Sugita, and Y. Okamoto, Biopolymers (Peptide Science) **60** (2001) 96–123.
[3] Y. Sugita and Y. Okamoto, in *Lecture Notes in Computational Science and Engineering*, edited by T. Schlick and H.H. Gan (Springer-Verlag, Berlin, 2002) pp. 304–332; e-print: cond-mat/0102296.
[4] B.A. Berg, Comp. Phys. Commun. **147** (2002) 52–57.
[5] Y. Sugita, A. Mitsutake, and Y. Okamoto, in *Lecture Notes in Physics*, edited by W. Janke (Springer-Verlag, Berlin, 2008) pp. 369–407.; e-print: arXiv:0707.3382v1 [cond-mat.stat-mech].
[6] A.M. Ferrenberg and R.H. Swendsen, Phys. Rev. Lett. **61** (1988) 2635–2638; *ibid.* **63** (1989) 1658.
[7] A.M. Ferrenberg and R.H. Swendsen, Phys. Rev. Lett. **63** (1989) 1195–1198.
[8] S. Kumar, D. Bouzida, R.H. Swendsen, P.A. Kollman, and J.M. Rosenberg, J. Comput. Chem. **13** (1992) 1011–1021.
[9] B.A. Berg and T. Neuhaus, Phys. Lett. **B267** (1991) 249–253.
[10] B.A. Berg and T. Neuhaus, Phys. Rev. Lett. **68** (1992) 9–12.
[11] A.P. Lyubartsev, A.A. Martinovski, S.V. Shevkunov, and P.N. Vorontsov-Velyaminov, J. Chem. Phys. **96** (1992) 1776–1783.
[12] E. Marinari and G. Parisi, Europhys. Lett. **19** (1992) 451–458.
[13] K. Hukushima and K. Nemoto, J. Phys. Soc. Jpn. **65** (1996) 1604–1608.
[14] C.J. Geyer, in *Computing Science and Statistics: Proc. 23rd Symp. on the Interface*, edited by E.M. Keramidas (Interface Foundation, Fairfax Station, 1991) pp. 156–163.
[15] F. Wang and D.P. Landau, Phys. Rev. Lett. **86** (2001) 2050–2053.
[16] F. Wang and D.P. Landau, Phys. Rev. E **64** (2001) 056101.
[17] E. Marinari, G. Parisi, and J.J. Ruiz-Lorenzo, in *Spin Glasses and Random Fields*, edited by A.P. Young (World Scientific, Singapore, 1998) pp. 59–98.
[18] U.H.E. Hansmann, Y. Okamoto, and F. Eisenmenger, Chem. Phys. Lett. **259** (1996) 321–330.
[19] N. Nakajima, H. Nakamura, and A. Kidera, J. Phys. Chem. B **101** (1997) 817–824.
[20] Y. Sugita and Y. Okamoto, Chem. Phys. Lett. **314** (1999) 141–151.
[21] B.A. Berg, U.H.E. Hansmann, and T. Neuhaus, Phys. Rev. B **47** (1993) 497–500.
[22] W. Janke and S. Kappler, Phys. Rev. Lett. **74** (1995) 212–215.
[23] S. Kumar, P. Payne, and M. Vásquez, J. Comput. Chem. **17** (1996) 1269–1275.
[24] C. Bartels and M. Karplus, J. Comput. Chem. **18** (1997) 1450–1462.
[25] Y. Iba, G. Chikenji, and M. Kikuchi, J. Phys. Soc. Jpn. **67** (1998) 3327–3330.
[26] B.A. Berg, H. Noguchi, and Y. Okamoto, Phys. Rev. E **68** (2003) 036126.
[27] S.G. Itoh and Y. Okamoto, Chem. Phys. Lett. **400** (2004) 308–313.
[28] J. Higo, N. Nakajima, H. Shirai, A. Kidera, and H. Nakamura, J. Comput. Chem. **18** (1997) 2086–2092.
[29] H. Okumura and Y. Okamoto, Chem. Phys. Lett. **383** (2004) 391–396.
[30] S.G. Itoh and Y. Okamoto, Mol. Sim. **33** (2007) 83–89.
[31] Y. Sugita, A. Kitao, and Y. Okamoto, J. Chem. Phys. **113** (2000) 6042–6051.
[32] T. Okabe, M. Kawata, Y. Okamoto, and M. Mikami, Chem. Phys. Lett. **335** (2001) 435–439.
[33] D. Paschek and A.E. Garcia, *Phys. Rev. Lett.* **93** (2004) 238105.
[34] A. Mitsutake and Y. Okamoto, Phys. Rev. E **79** (2009) 047701.
[35] A. Mitsutake and Y. Okamoto, J. Chem. Phys. **130** (2009) 214105.
[36] A. Mitsutake, J. Chem. Phys. **131** (2009) 094105.
[37] Y. Mori and Y. Okamoto, submitted for publication; e-print: arXiv:1004.2076v1 [cond-mat.stat-mech].
[38] G.M. Torrie and J.P. Valleau, J. Comput. Phys. **23** (1977) 187–199.
[39] Y. Sugita and Y. Okamoto, Chem. Phys. Lett. **329** (2000) 261–270.
[40] A. Mitsutake and Y. Okamoto, Chem. Phys. Lett. **332** (2000) 131–138.
[41] A. Mitsutake, Y. Sugita, and Y. Okamoto, J. Chem. Phys. **118** (2003) 6664–6675.
[42] A. Mitsutake, Y. Sugita, and Y. Okamoto, J. Chem. Phys. **118** (2003) 6676–6688.

[43] A. Mitsutake and Y. Okamoto, J. Chem. Phys. **121** (2004) 2491–2504.
[44] I. R. McDonald, Mol. Phys. **23** (1972) 41.
[45] H. Okumura and Y. Okamoto, Chem. Phys. Lett. **383** (2004) 391.
[46] H. Okumura and Y. Okamoto, Phys. Rev. E **70** (2004) 026702.
[47] G. J. Martyna, D. J. Tobias, and M. L. Klein, J. Chem. Phys. **101** (1994) 4177.
[48] S. Nosé, Mol. Phys. **52** (1984) 255.
[49] S. Nosé, J. Chem. Phys. **81** (1984) 511.
[50] W. G. Hoover, Phys. Rev. A **31** (1985) 1695.
[51] H. C. Andersen, J. Chem. Phys. **72** (1980) 2384.
[52] J.K. Myers, C.N. Pace, and J.M. Scholtz, Proc. Natl. Acad. Sci. U.S.A. **94**, 2833–2837 (1997).
[53] F.A. Momany, R.F. McGuire, A.W. Burgess, and H.A. Scheraga, J. Phys. Chem. **79** (1975) 2361.
[54] G. Némethy, M.S. Pottle, and H.A. Scheraga, J. Phys. Chem. **87** (1983) 1883.
[55] M.J. Sippl, G. Némethy, and H.A. Scheraga, J. Phys. Chem. **88** (1984) 6231.
[56] T. Ooi, M. Oobatake, G. Némethy, and H.A. Scheraga, Proc. Natl. Acad. Sci. USA **84** (1987) 3086–3090.
[57] M. Masuya, unpublished; see http://biocomputing.cc/nsol/.
[58] H. Kawai, Y. Okamoto, M. Fukugita, T. Nakazawa, and T. Kikuchi, Chem. Lett. **1991** (1991) 213–216.
[59] Y. Okamoto, M. Fukugita, T. Nakazawa, and H. Kawai, Protein Eng. **4** (1991) 639–647.
[60] W. Humphrey, A. Dalke, and K. Schulten, J. Mol. Graph. Mod. **14** (1996) 33–38.
[61] E.A. Merritt and D.J. Bacon, Methods in Enzymology **277** (1997) 505–524.
[62] J. W. Ponder and F. M. Richards, J. Comput. Chem. **8** (1987) 1016.
[63] J. Wang, P. Cieplak, and P. A. Kollman, J. Comput. Chem. **21** (2000) 1049.
[64] W. L. Jorgensen, J. Chandrasekhar, J. D. Madura, R. W. Impey, and M. L. Klein, J. Chem. Phys. **79** (1983) 926.
[65] T. Darden, D. York, and L. Pedersen, J. Chem. Phys. **98** (1993) 10089.
[66] U. Essmann, L. Perera, M. L. Berkowitz, T. Darden, H. Lee, and L. G. Pedersen, J. Chem. Phys. **103** (1995) 8577.
[67] G. J. Martyna, M. E. Tuckerman, D. J. Tobias, and M. L. Klein, Mol. Phys. **87** (1996) 1117.
[68] J.-P. Ryckaert, G. Ciccotti, and H. J. C. Berendsen, J. Comput. Phys. **23** (1977) 327.
[69] H. C. Andersen, J. Comput. Phys. **52** (1983) 24.
[70] H. Okumura and Y. Okamoto, Bull. Chem. Soc. Jpn. **80** (2007) 1114.
[71] H. Okumura and Y. Okamoto, J. Phys. Chem. B **112** (2008) 12038.